Spatial Variability of Atmospheric Boundary Layer Structure over the Eastern Equatorial Pacific

BINGFAN YIN AND BRUCE A. ALBRECHT

Rosenstiel School of Marine and Atmospheric Sciences, University of Miami, Miami, Florida

(Manuscript received 12 November 1998, in final form 14 April 1999)

ABSTRACT

Variations in the atmospheric boundary layer structure over the eastern equatorial Pacific are analyzed using 916 soundings collected during the First Global Atmospheric Research Program Global Experiment. Unstable boundary layer structures are observed much more frequently in soundings north of the ocean front located near 2.5°N in the eastern equatorial Pacific than in soundings south of the front. An objective criterion is applied to identify the presence of the transition layer, a weak stable layer near cloud base, in the soundings. The transition is observed in about 45% of the soundings in both the unstable and the inversion categories. A comparison of soundings over the cold tongue with those over the ITCZ indicates that differences in static stability between these regions are limited to the layer from the surface to about 850 mb, which is the mean height of the inversions capping the cloud layer over the cold tongue. The cold tongue soundings on average are found to be drier from the surface to 300 mb than the ITCZ soundings with the largest average difference ($\sim$5 g kg^{-1}) between these two groups of soundings observed just above the inversion layer. Compensating subsidence from the ITCZ may account for some of the drying observed just above the cold tongue inversions, although horizontal advection may also be a factor. North–south cross sections (10°S–15°N) of potential temperature, mixing ratio, equivalent potential temperature, and meridional wind across the cold tongue–ITCZ complex (CTIC) were constructed for two longitudinal bands: 95°–105°W and 105°–115°W. There is little latitudinal variation of the average height of the trade inversion and the height of the transition layer across the CTIC. Although the average lifting condensation level (LCL) at 980 mb is located near the average top of the transition layers observed over the cold tongue, the average 980-mb LCL is close to the average height of the base of the transition layers observed over the ITCZ. These differences, while subtle, may have a substantial impact on the coupling between the subcloud and the cloud layer in these two regions. Strong boundary layer meridional winds are observed near the surface at about 7.5°N over the higher SSTs north of the cold tongue. The average meridional winds over the cold tongue show little vertical shear over the lowest 100 mb of the boundary layer.

1. Introduction

Air–sea interaction over the eastern equatorial Pacific cold tongue and intertropical convergence zone (ITCZ) complex (CTIC) must be well understood to predict the El Niño–Southern Oscillation over the Pacific Ocean and its effects on weather and climate of remote regions with quantitative accuracy. The variability of the CTIC structure depends on the strength of the coupling between the ocean and atmosphere. Factors that control the strength of this coupling are believed to include the distribution of the sea surface temperature (SST) along the equator and the magnitude of the wind stress forcing (Neelin 1990; Meehl 1990), both of which are intimately connected to the structure of the marine atmospheric boundary layer (MABL). Coupled models tend to produce unrealistic symmetric ITCZs and unrealistic atmospheric boundary layer structures over the cold tongue (Mechoso et al. 1995); consequently it is necessary to improve our understanding of the eastern Pacific ocean–atmosphere coupling.

In the eastern equatorial Pacific, prominent features of the mean SST distribution are the equatorial cold tongue, which extends along the equator from the coast of South America westward to about 160°W, and the equatorial front, which is located slightly north of the equator (Wallace et al. 1989). The prevailing southeasterly winds accelerate as they cross the equatorial front, and the ITCZ is located where these southeasterly winds weaken. Climatologically, the location of the ITCZ over the eastern equatorial Pacific shifts between about 5°N in January and 15°N in July. At the surface, wind speeds increase as the air passes over the ocean front from the cold tongue to the warmer water north of the equator (Hayes et al. 1989). However, unless constrained by observations, models tend to underestimate the directional shear and the equatorial asym-

Corresponding author address: Dr. Bruce A. Albrecht, RSMAS/MPO, University of Miami, 4600 Rickenbacker Causeway, Miami, FL 33149-1098.
E-mail: balbrecht@rsmas.miami.edu

metry in the surface winds in this region (Latif et al. 1990). Previous studies suggested that at least two processes might play roles in the dynamics of the surface wind fields near the equator. Lindzen and Nigam (1987) suggested that the seasonal and interannual variability of surface wind is due, in part, to hydrostatic sea level pressure changes induced by changes in the strength of the cold tongue. The other important factor is related to atmospheric boundary layer processes. Wallace et al. (1989) argued that as air passes from the cold tongue to the warmer waters north of the equator, the boundary layer becomes more unstable, the wind shear in the boundary layer is reduced, and hence surface wind speeds increase. The steady flows across the SST gradients associated with the CTIC results in variations in cloud and boundary layer structure that are neither easily modeled nor parameterized.

To test Wallace's hypothesis, Bond (1992) analyzed the planetary boundary layer structure over the eastern equatorial Pacific using 68 soundings collected along a 110°W north–south transect made with the research ship *Discoverer* in 1989. He found significant boundary layer variability due to cloud cover, synoptic-scale variability, and diurnal effects. There were, however, systematic variations in the mean structure of the mixed layer as a function of latitude. These observations indicated that the mixed layer was neutrally stratified over warm water between 6.5° and 1.5°N and was slightly stably stratified over the cooler water between 1°N and 2°S. The Bond (1992) observations are consistent with the hypothesis proposed by Wallace et al. (1989) and Hayes et al. (1989) that the low-level wind shear was enhanced on the cold side of the SST front because of greater static stability in this area than over the equatorial front.

Using data collected in the First Global Atmospheric Research Program (GARP) Global Experiment (FGGE) in 1979, Kloesel and Albrecht (1989; KA89 hereinafter) studied the structure of the boundary layer over a broad region of the equatorial Pacific. They found that low-level inversions of sufficient strength to inhibit deep convection were present in more than 50% of the soundings. These inversions appear to play a critical role in regulating convective activity over the central and eastern Pacific. The tops of the inversions have an average pressure level of approximately 800 mb and show little latitudinal variation. Observational studies (Augstein et al. 1974; Fitzjarrald and Garstang 1981; Nicholls 1984; Paluch and Lenschow 1991; Albrecht et al. 1995a) indicate that under many circumstances MABLs are characterized by a decoupled boundary layer. Under these conditions a weak inversion, the transition layer, separates the cloud layer from the subcloud layer as shown in Fig. 1. This results in a relatively sharp decrease in mixing ratio across the transition layer. The transition layer regulates the nature and magnitude of transports from the subcloud to the cloud layer (Betts 1976; Nicholls and LeMone 1980; Fitzjarrald and Garstang 1981). However, there have been relatively few studies of the transition layer processes in equatorial regions since the GARP Atlantic Tropical Experiment (1974). In this study, we develop an objective criterion to identify a transition layer in individual soundings and then use a layer-to-layer averaging approach to develop composite soundings that maintain the details of both the transition layer and the higher-level trade inversion if it is present in the sounding. In this paper we define the marine atmospheric boundary layer as the layer that extends from the surface to the top of the trade inversion. The layer below the transition layer will be called the subcloud layer. Although this is layer often called the mixed layer, this terminology can be misleading since the water vapor mixing ratio is rarely completely mixed in this layer.

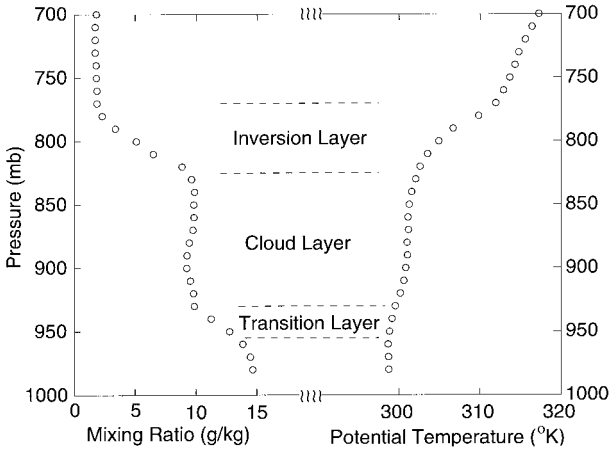

FIG. 1. A typical sounding illustrating the trade inversion and boundary layer structure. The sounding was made at 1800 UTC 1 Jun 1979, at 108.8°W and 5.9°S during FGGE. The transition layer is clearly indicated by a decrease in moisture and an increase in potential temperature at about 950 mb.

Despite the importance of the MABL over the eastern equatorial Pacific, observational studies are relatively limited because of its remoteness. Some early studies of cloud and layer structure across the CTIC were made using aircraft (Albert 1946) and soundings obtained from ships transecting the equator in the eastern Pacific (Neiburger et al. 1961). More recent studies of the MABL over the eastern equatorial Pacific focused mainly on the mean structure and the mixed layer variability (KA89; Bond 1992). It is necessary, however, to expand upon these studies to describe the detailed evolution of boundary layer across the CTIC. In this paper, soundings collected during FGGE are used to analyze the spatial variability in atmospheric boundary structures over the eastern equatorial Pacific. These FGGE observations are of particular interest since they are made over a relatively broad region of the eastern and central equatorial Pacific. Although detailed studies of boundary layer structure have been made with portions of the FGGE datasets (KA89; Firestone and Albrecht 1986; Betts and Albrecht 1987), the evolution of the boundary layer over

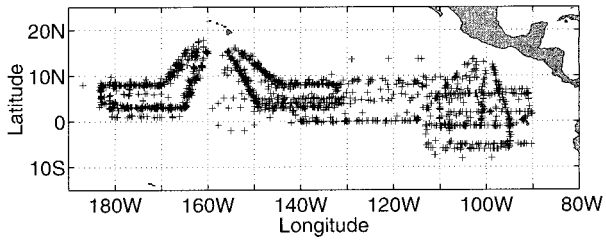

FIG. 2. Scatterplot of locations of soundings launched during both SOP-I and SOP-II of FGGE.

the CTIC has not been well documented. In this paper we focus on the structure and frequency of trade inversions and transition layer structures in the eastern equatorial Pacific and the variation of boundary layer structure across the CTIC.

In section 2 the datasets and the methods used to analyze the data are described. Documentation of the boundary layer structures observed over the eastern Pacific is presented in section 3. A comparison of the atmospheric boundary layer between the cold tongue and the ITCZ is presented in section 4. The variations in boundary layer structure over the eastern equatorial Pacific are documented in section 5. In section 6 conclusions and a general discussion of the processes responsible for the variations in boundary layer structure over the region are presented.

2. Description of data

Three principal sources of data were used for this study: FGGE soundings, mean SST, and outgoing longwave radiation (OLR) fields. Figure 2 shows where the FGGE soundings were launched. A detailed description of sounding data collected during FGGE can be found in KA89. A total of about 1500 soundings were collected in the area from 160° to 90°W, 10°S to 15°N during FGGE. A subset of these (~900) are used to analyze the boundary layer structure over the central and eastern equatorial Pacific. Some of the FGGE soundings collected west of this area were also used for comparison purposes.

The individual soundings were analyzed following the procedure described in KA89. The data used in this study are the temperature, humidity, and horizontal winds at 10-mb pressure levels from 300 to 980 mb. Many of the FGGE soundings did not have data for pressures greater than 980 mb.

The SST datasets were derived from in situ marine surface observations as reported on the Global Telecommunication System (Reynolds and Gemmill 1984). The resolution of the SST data is 2° in both latitude and longitude. Mean SST fields for January and February and May and June in 1979 are shown in Figs. 3a and 3b, respectively. The SST distributions show the western Pacific warm pool extending farther eastward and SSTs north of the equator in the eastern Pacific appearing much warmer during May and June than during January and February in 1979. In the eastern Pacific, the equatorial cold tongue was centered slightly south of the equator and the warmest SSTs were centered at about 10°N, 100°W. During May and June, SSTs were higher in the whole domain and the warm center at about 10°N, 100°W was stretched out in the east–west direction. The eastern Pacific cold tongue became narrow, and the ocean front north of the cold tongue was much more clearly defined during May and June than during January and February.

The presence of deep convection in the study area was identified using OLRs from satellite observations. The OLR dataset used in this study is based on observations from the National Oceanic and Atmospheric Administration's polar-orbiting satellites (Gruber and Krueger 1984). This dataset was produced from daytime and nighttime archived OLR estimations interpolated onto a 2.5° × 2.5° grid globally. Figures 4a and 4b show the mean OLR fields for January and February, and May and June in 1979. The location of deep convection associated with the ITCZ is marked by low values of OLR. High values of OLR south of the equator are associated with the divergent southeasterly flow south in this region. The most likely type of clouds in this area would be fair-weather cumulus (Norris 1998). The OLR distributions indicate that from 160°E to 120°W the ITCZ, as defined by high clouds, was located between 10°N and the equator during January and February and shifted to about 10°N during May and June. In the eastern equa-

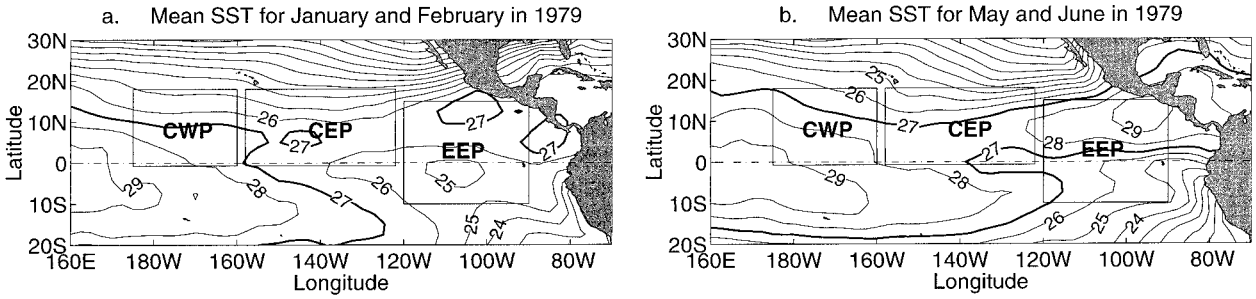

FIG. 3. Mean SST for (a) Jan and Feb, and (b) May and Jun in 1979. Solid boxes indicate the FGGE study regions. The value of the thick contour is 27°C and the contour interval is 1°C.

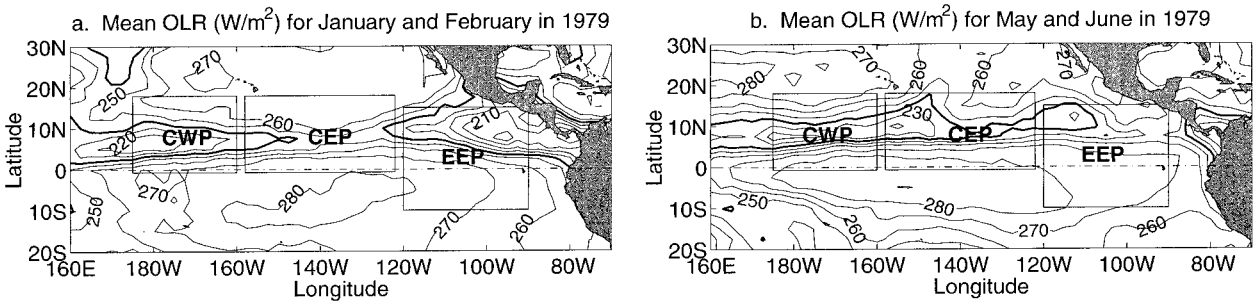

FIG. 4. Mean OLR for (a) Jan and Feb, and (b) May and Jun in 1979. Solid boxes indicate the FGGE study regions. The value of the thick contour is 240 W m^{-2} and the contour interval is 10 W m^{-2}.

torial Pacific, the low OLRs centered at 10°N, 100°W during January and February shifted westward approximately 5° during May and June, and the values at the low OLR center increased. The threshold used to identify areas of deep convection is typically suggested to be in the range of 240–260 W m^{-2} (Lau and Chan 1983; Waliser et al. 1993). However, any threshold will be subject to regional biases (Waliser et al. 1993).

Data from the soundings were subjected to an objective quality control procedure to eliminate questionable data. As part of this procedure, averages of the temperature and the mixing ratio were calculated at each pressure level from 980 to 300 mb for soundings in the three regions (eastern equatorial Pacific, EEP; central eastern Pacific, CEP; and central western Pacific, CWP) shown in Fig. 3. Individual values of the temperature or the mixing ratio that differed by more than three standard deviations from the means were eliminated. The remaining soundings were then subjected to this procedure for a second time. In addition, soundings with unreliable relative humidity (RH) or wind profiles, for instance, 100% RH at every pressure level, were also eliminated. A total of 916 FGGE soundings remained in the EEP and CEP datasets after this data quality control procedure was applied. Although the expected accuracy of 1°C for temperature and 5% for relative humidity (KA89) may be appropriate under clear-sky conditions, the sensors are known to give systematic errors when a sonde enters the cloud and for some time after it falls out of the cloud. The data screening technique that we have applied is meant to identify the bulk of the soundings that may be affected by such errors.

3. MABL structures over the eastern equatorial Pacific

a. Composite soundings and statistics on sounding structures

To describe the variability of MABL structure over the study area, soundings were classified on the basis of low-level stability. The classification criteria used in this study are similar to those used in KA89. Since a nonentraining parcel rising pesudoadiabatically from the surface will conserve equivalent potential temperature θ_e, the θ_e near the surface was compared with the saturation equivalent potential temperature θ_{es} at higher levels to estimate the buoyancy of the parcel. This approach provides an easy visualization of parcel buoyancy as defined by the temperature difference between the rising parcel and the environment (e.g., Bohren and Albrecht 1998). The effects of water vapor and liquid water on the buoyancy were neglected for this simple classification, although these effects cannot be neglected when quantifying convective available potential energy (e.g., Xu and Emanuel 1989; Emanuel 1994; Williams and Renno 1993).

Since a number of the FGGE soundings (~23%) did not have data at pressures greater than 980 mb, the stability classification was made using air parcels originating from 980 mb instead of from a lower level. If θ_e at 980 mb was greater than θ_{es} above the lifting condensation level (LCL) but intersected the θ_{es} profile at a pressure level below 600 mb, the sounding was classified as an inversion sounding. The intersection of the θ_e path ascending from 980 mb and the θ_{es} profile suggests that a stable layer (the inversion layer) exists above the unstable layer. The LCL used here is the LCL of air at 980 mb. The remaining soundings were then divided into three groups. If a parcel rising from 980 mb was positively buoyant (θ_e at 980 mb $>$ θ_{es}) above the LCL to at least the 600-mb level, the sounding was classified as unstable. The positive buoyancy indicates that a nonentraining rising parcel will accelerate, which is favorable for the development of deep convection. Soundings with levels of free convection (LFCs) less than 100 mb from the LCLs were also classified as unstable soundings. The LFC here is determined as the level where θ_{es} is equal to the value of θ_e at 980 mb. If the low-level parcel was negatively buoyant (θ_e at 980 mb $\leq$ θ_{es}) to the 600-mb level, the sounding was classified as deep stable. If the parcel was negatively buoyant to a level below 600 mb, the sounding was classified as stable. In this study, deep stable soundings and stable soundings are combined into one group, the stable group, since there are relatively few soundings in these two categories. The average SST for the stable group

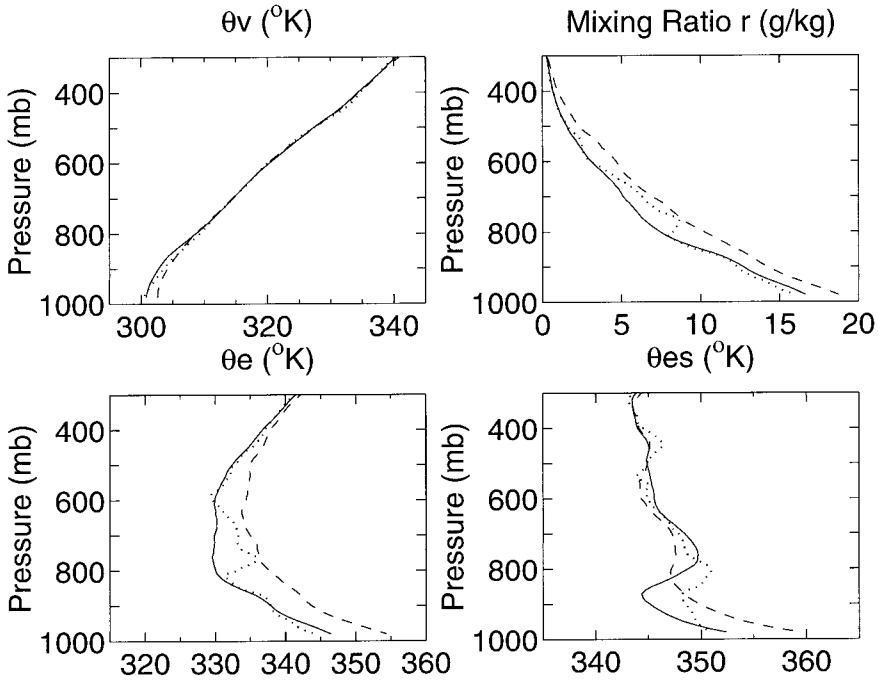

FIG. 5. Mean potential temperatures and mixing ratio for stable, inversion, and unstable categories over EEP during both SOP-I and SOP-II. Dotted line: stable, 23 soundings; thin solid line: inversion, 270 soundings; broken line: unstable, 160 soundings. The freezing level is located at ~570 mb.

in the EEP area is about 0.5°C less than the average SST for the unstable group.

During the two FGGE observation periods SOP-I and SOP-II, a total of 676 dropwinsondes were launched over the eastern equatorial Pacific (EEP in Fig. 3 for SOP-I and SOP-II), and 453 soundings remained after the data quality control procedure was applied. Of these remaining soundings 60% had inversion layers; 5% had stable boundary layer structures and the remaining 35% were classified as unstable boundary layers. These statistics may be biased in favor of the stable soundings (both the inversion and stable groups) since the aircraft that deployed the dropwinsondes avoided the areas of deepest convection. In addition, in the present study soundings with LFCs less than 100 mb from LCLs were classified as unstable soundings. If the soundings are classified by specifying that the LFC be no more than 50 mb above the LCL, the percentage of inversion (unstable) soundings increases (decreases) by about 3%. The classification of soundings is also sensitive to the level used to define the initial parcel characteristics. To estimate this sensitivity, the soundings were also classified by extrapolating temperatures and mixing ratios from 980 to 1010 mb and then using 1010 mb as the parcel starting level. The temperature extrapolation was made by assuming the potential temperature from 980 to 1010 mb is well mixed. The average mixing ratio variation with height obtained from soundings that made it to pressures greater than 980 mb was used to extrapolate the mixing ratios to 1010 mb for each sounding. The classifications obtained using θ_e at 1010 mb rather than 980 mb reduces the percentage of inversion soundings from about 60% to about 55% with a corresponding increase in the number of unstable soundings.

Figure 5 shows the profiles of average virtual potential temperature (θ_v), mixing ratio (r), θ_e, and θ_{es} for unstable, inversion, and stable soundings over the eastern equatorial Pacific during both SOP-I and SOP-II. Profiles of θ_v show that the subcloud layer for unstable soundings is warmer than those for the inversion and stable soundings, while above 800 mb the three curves are almost identical. Since the average SSTs for the inversion and stable soundings are about 0.5°C less than that for the unstable soundings, it is apparent that many of the inversion and stable soundings occur over the lower SSTs to the south of the ITCZ. Profiles of mixing ratio indicate that the unstable composite sounding is more moist than the inversion and the stable soundings; this is consistent with moistening of the upper levels due to the deeper moist convection associated with the unstable boundary layers. In addition, a humidity reversal (KA89) is clearly indicated just above 800 mb in the average mixing ratio of stable soundings. The average profile of θ_{es} for the inversion soundings show a well-defined inversion layer despite the smoothing caused by the averaging procedure. These inversion layers are strong enough to inhibit deep convection, even though the temperature differences between the unstable and inversion composite soundings are small. Although the averaged unstable sounding does not show a similar

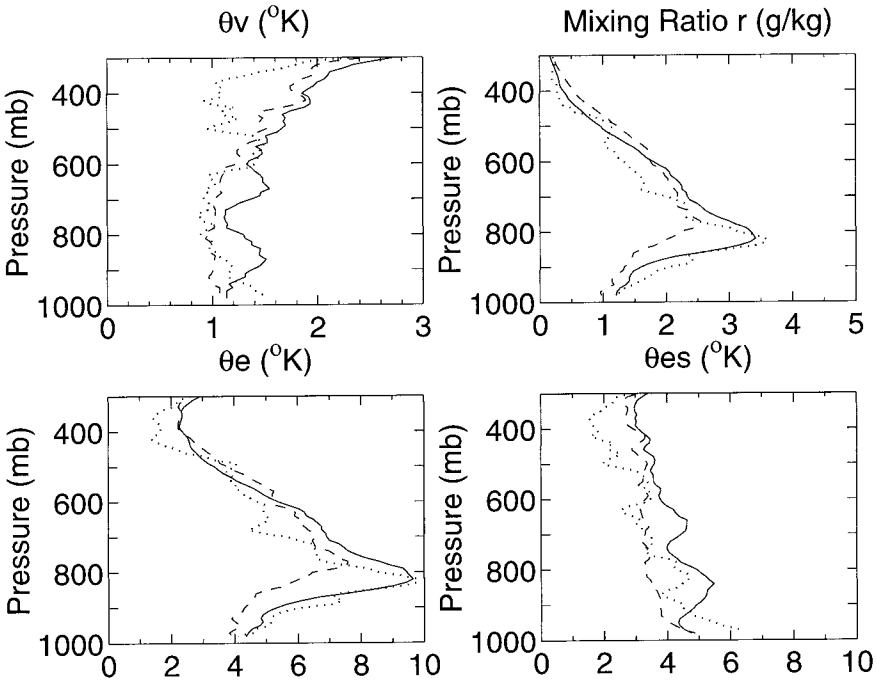

FIG. 6. Standard deviations of the variables in Fig. 5.

stable layer, there is a layer where $\partial\theta_{es}/\partial z \approx 0$ between 800 and 700 mb. This layer is present since some of the soundings in the unstable group include inversions that are not strong enough to merit the inversion classification. These soundings may represent a transition between the stable and unstable boundary layers. It is also found that in most of cases in the unstable category there are inversion layers around the freezing level (~570 mb). Johnson et al. (1996) suggest that these inversion layers result from melting effects in precipitating systems. There is no stable layer at the freezing level in the inversion composite sounding shown in Fig. 5, which is consistent with the suppression of deep convection and a lack of freezing level processes for this case.

To quantify the variability associated with each variable for the three convective classifications, the standard deviation was calculated (Fig. 6). The temperature variability is smallest in the lowest 200 mb. There is a pronounced peak in the mixing ratio variability near the base of the trade inversion that is defined in the stable and the unstable soundings. The standard deviation of the mixing ratio associated with the unstable sounding is a maximum near 800 mb, which is near the base of a slightly stable layer that is observed in the mean unstable sounding (Fig. 5).

Table 1 shows the mean top and base of the inversion layers for soundings over the eastern equatorial Pacific during SOP-I and SOP-II. The inversion top is defined by the location of the maximum in the θ_{es} profile. The inversion base is defined at the level where the sign of the vertical gradient of θ_{es} changes from positive to negative below the inversion top. For soundings containing multiple inversions, the inversion with the largest difference in θ between inversion top and base was identified as the principal inversion layer. The average tops of inversion layers over the eastern equatorial Pacific were at approximately 770 mb and the average inversion base was located at about 850 mb. Most of the inversion soundings had inversion bases ranging from 950 to 800

TABLE 1. Statistics of inversion soundings over the EEP during SOP-I and SOP-II. Here $\Delta\theta$, $\Delta\theta_v$, $\Delta\theta_e$, and Δr are differences in θ, θ_v, θ_{es}, and r between the top and the base of the inversion layer. Std devs are indicated by $\pm$ values.

	SOP-I	SOP-II	Total
Inversion soundings	114	156	270
Inversion base (mb)	838 ± 57	858 ± 52	849 ± 55
Inversion top (mb)	761 ± 70	777 ± 56	770 ± 63
Thickness (mb)	77 ± 44	81 ± 41	79 ± 41
$\Delta\theta$ (K)	6.93 ± 3.15	8.36 ± 3.25	7.77 ± 3.28
$\Delta\theta_v$ (K)	6.18 ± 2.88	7.28 ± 2.95	6.82 ± 2.97
$\Delta\theta_e$ (K)	−5.17 ± 6.46	−9.18 ± 7.34	−7.48 ± 7.25
Δr (g kg^{-1})	−4.28 ± 2.67	−6.16 ± 3.02	−5.37 ± 3.02

mb and inversion tops ranging from 850 to 700 mb. Table 1 indicates that the inversion layer was slightly higher during SOP-I (average SST 25.9°C) than during SOP-II (average SST 26.8°C) and that the decrease in mixing ratio across the inversion was greater during SOP-II than during SOP-I. The interpretation of these results is complicated, however, because of the wide range of geographical locations of the soundings.

The unstable soundings from 7.5°S to the equator were fewer than 20% of the total soundings in this region, while from 2.5° to 12.5°N more than 40% of the soundings were classified as unstable. The longitudinal differences in the percentage of the three categories of soundings are not significant. As expected, the statistics indicate that as the SSTs increase from south to north, the atmospheric boundary layers become more unstable, as indicated by fewer inversions. Although the unstable soundings during SOP-II are generally observed over SSTs greater than 27°C, stable and inversion soundings are observed over the full range of SSTs that were observed in the study area.

b. Transition layer structure and statistics

Although the composite soundings over the eastern Pacific indicate the importance of inversions near 800 mb in regulating the potential for deep convection, the transition layer may be critical for the moisture and heat exchange between the cloud and the subcloud layer. An example of the profiles of mixing ratio and potential temperature for a typical sounding in which the transition layer is present is shown in Fig. 1. The transition layer is indicated by the rapid decrease in mixing ratio and the increase in potential temperature near 950 mb. Previous observational studies (Augstein et al. 1974; Betts 1976; Nicholls and LeMone 1980; Fitzjarrald and Garstang 1981; Nicholls 1984; Paluch and Lenschow 1991; Albrecht et al. 1995a) show that the transition layer is key in controlling the convective mass transport between the subcloud and the cloud layer.

To generate statistics on the occurrence of the transition layer during FGGE, both the unstable and the inversion soundings were separated into those with and those without a transition layer. Across the transition layer, the potential temperature θ increases and the mixing ratio r decreases rapidly with height. These changes, however, are generally much smaller than the changes across the 800-mb trade inversion that caps the cloud layer, and thus they are more difficult to identify. The decrease in mixing ratio at the transition layer contributes to a reduction in the θ_v increase across the transition layer. To help identify these relatively subtle layers in a sounding, a parameter $\mu = -(\partial\theta/\partial p - \beta\partial r/\partial p)$ was defined to establish an objective method for screening the soundings. The β in the expression for μ is chosen to convert $\partial r/\partial p$ to the same units as $\partial\theta/\partial p$ by considering the effects of these two terms on the vertical gradient of θ_v. Since $\theta_v = \theta(1 + 0.608r)$, $\beta = 0.608\theta/(1 + 0.608r)$ will give $\beta\partial r/\partial p$ the proper units. In general the mixing ratio term in the expression for μ will contribute less to μ than the potential temperature term. Although other weightings of the θ and r gradients could be devised, we use a weighting that depends on the contributions of the individual θ and r gradients to density gradients.

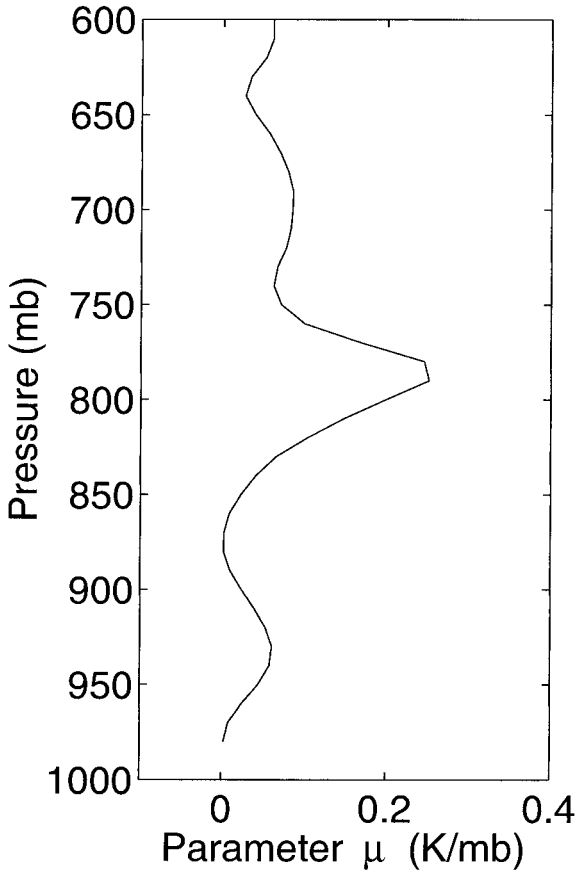

FIG. 7. Vertical profile of μ of the sounding that has the transition layer near 930 mb shown in Fig. 1.

To illustrate μ and how it relates to the thermodynamic structure, the vertical profile of μ of the typical transition layer sounding shown in Fig. 1 is shown in Fig. 7. The transition layer is clearly indicated by a local maximum of μ at about 930 mb. Before calculating the vertical gradient of θ and r needed to calculate μ, a 1–2–1 smoother was applied to θ and r at each sounding level to give smooth local gradients that can be used to test objectively for the presence of transition layers.

The ratio $\lambda \equiv \mu/\overline{\mu}$ was used to determine objectively whether a transition layer was present, where $\overline{\mu}$ is the average for μ from 980 to 900 mb of an individual sounding. This pressure interval is chosen since usually the much stronger trade wind inversion is located at pressures less than 900 mb. If at some pressure level between 980 and 900 mb λ is equal to or greater than 1.3, the sounding is classified as a transition layer sound-

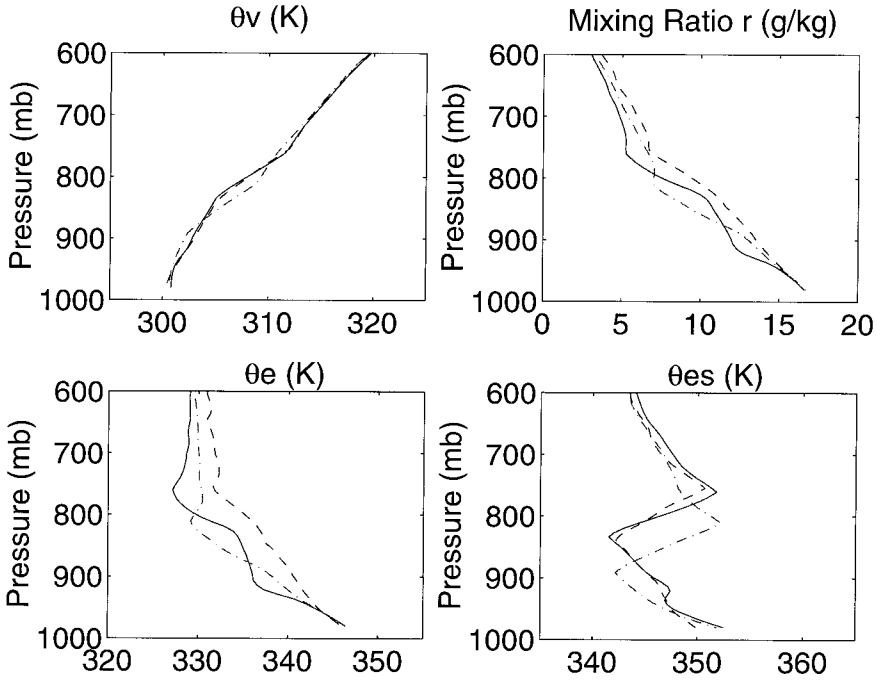

FIG. 8. Profiles of averaged θ_v, r, θ_e, and θ_{es} for soundings with different λ. The three composite soundings were made from all FGGE soundings that have inversion layers using the layer-by-layer average procedure; $\lambda > 1.3$: solid line, 317 soundings; $1 < \lambda \leq 1.3$: broken line, 65 soundings; $\lambda \leq 1.0$: dot–dashed line, 256 soundings.

ing, provided it is below the base of the trade inversion. Since low trade inversions can affect the value of $\overline{\mu}$ it is possible to have λ less than 1. The thickness of the transition layer is that of the layer in which λ is equal to or greater than 1.3. This specific value of λ was chosen to provide an objective selection of transition layer soundings that was consistent with a subjective, manual identification of these layers. To illustrate how this value was selected, averaged profiles of θ_v, r, θ_e, θ_{es} for inversion soundings with three different ranges of λ are illustrated in Fig. 8. Here the decoupling below 900 mb is much more clearly defined in soundings with λ greater than 1.3. Thus $\lambda \geq 1.3$ is chosen as the threshold value of λ to identify soundings with transition layers.

The profiles shown in Fig. 8 are obtained by a layer-by-layer averaging procedure to prevent the transition layer structure from being smeared out by using the conventional average at each pressure level. The procedure is similar to that applied by Augstein et al. (1974) and considers the averages in temperature, mixing ratio, and other variables within five layers: subcloud layer, transition layer, cloud layer, inversion layer, and the layer above the inversion layer. A nondimensional scale is used within each of these layers. Layer averages using the nondimensional heights are then made and the resulting layer structures are converted to a dimensional height scale using the average height of each layer boundary. This procedure preserves the structure of the transition layer even if its height varies from sounding to sounding.

The frequency of occurrence of transition layers and the mean top and base of transition layers over the eastern equatorial Pacific during SOP-I and SOP-II are shown in Table 2. Of the total 453 soundings over the eastern equatorial Pacific, there are 203 (44.8%) soundings in which transition layers were present. The transition layers have an average base pressure level at approximately 943 mb with the standard deviation of 19 mb and an average top at 914 mb with a standard deviation of 24 mb. The LCLs for the 980-mb air of the transition soundings have an average pressure of 930 mb and were located within the transition layer in most of the soundings. The percentage of soundings with a transition layer is about the same for both the inversion and unstable group.

The transition layer is often most easily identified by a sharp decrease (negative jump) in mixing ratio near the cloud base. Although the negative jump in mixing ratio decreases the virtual potential temperature jump $\Delta\theta_v$, $\Delta\theta_v$ remains positive and is about 1°C. The differences in θ_e between the top and the base of the transition layer were negative and had an average of approximately -4 K; $\Delta\theta_v$ and $\Delta\theta_e$ show little variation during the SOP-I and SOP-II. East–west variations in the transition layer characteristics were obtained by calculating averages of $\Delta\theta_v$ for each of the three regions shown in Fig. 3 for both SOP-I and SOP-II. These re-

TABLE 2. Statistics for transition layer soundings over EEP during FGGE. Here $\Delta\theta$, $\Delta\theta_v$, $\Delta\theta_e$, and Δr are differences in θ, θ_v, θ_{es}, and r between the top and the base of the transition layer. The LCL pressure is for an air parcel at 980 mb. Std devs are indicated by ± values.

	SOP-I	SOP-II	Total
Occurrence of transition	48.3%	42.1%	44.8%
Transition soundings	97	106	203
Transition base (mb)	942 ± 20	944 ± 19	943 ± 19
Transition top (mb)	914 ± 24	913 ± 24	914 ± 24
LCL (mb)	933 ± 12	928 ± 16	930 ± 14
Thickness (mb)	28 ± 8	31 ± 11	29 ± 10
$\Delta\theta$ (K)	1.23 ± 0.63	1.20 ± 0.77	1.21 ± 0.71
$\Delta\theta_v$ (K)	0.91 ± 0.62	0.87 ± 0.71	0.89 ± 0.67
$\Delta\theta_e$ (K)	−3.97 ± 4.08	−4.21 ± 3.68	−4.10 ± 3.87
Δr (g kg^{-1})	−1.84 ± 1.42	−1.91 ± 1.34	−1.88 ± 1.38

sults give $\Delta\theta_v$ for the transition layer that varies from 0.89 to 0.93 K, which indicates the constancy of the transition layer structure over the eastern and central equatorial Pacific.

The differences between the thermodynamic structures of inversion soundings with and without the transition layers can be seen by comparing the composite sounding obtained with $\lambda < 1.0$ and $\lambda > 1.3$ in Fig. 8. The soundings without transition layers have a capping inversion with a base at 900 mb compared with about 840 mb for the transition layer soundings. The boundary layer structure near the surface, however, is nearly identical for the two cases.

A more detailed comparison was made for the transition and nontransition soundings using only SOP-II soundings to eliminate any seasonal variations. The two composite soundings (Fig. 9) were obtained by the layer-by-layer averaging procedure for inversion soundings with $\lambda \geq 1.3$ and those with λ less than 1.3. Profiles of θ_v indicate that soundings without the transition layers were slightly better mixed below the inversion layer (980–880 mb) than the transition soundings. In the cloud layer (940–880 mb), the nontransition soundings are moister than the transition sounding. This difference implies that the transition layer could play a role in regulating the transport of moisture from the subcloud layer to the cloud layer. For this SOP-II comparison, the profiles of θ_{es} indicate that the average trade inversion base for the transition soundings is only slightly higher than that of the nontransition soundings (840–860 mb). The more stringent condition of $\lambda < 1.0$ applied to all soundings to give the composite shown in

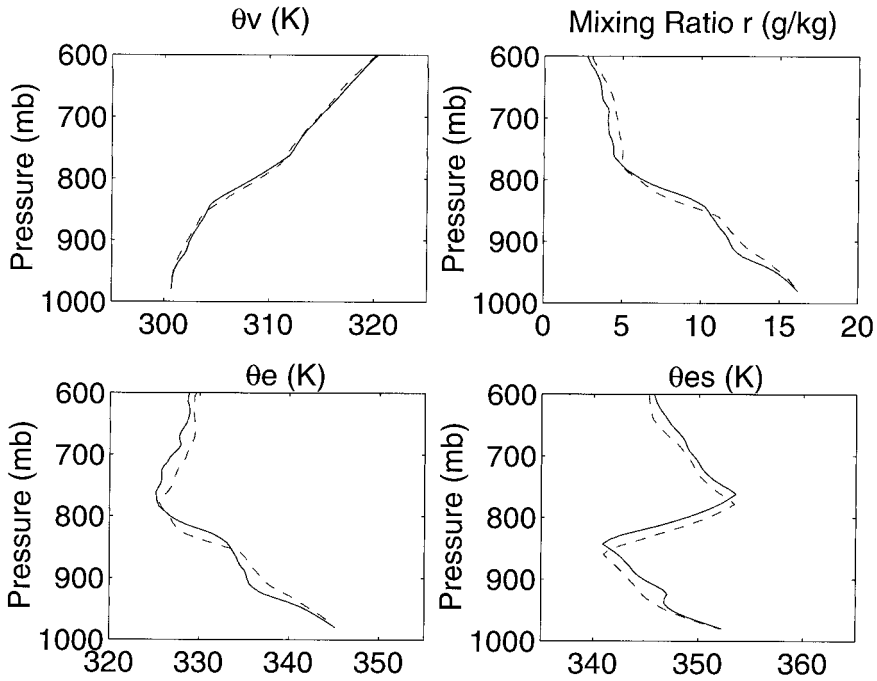

FIG. 9. Mean potential temperatures and mixing ratio for soundings with (solid line) and without (broken line) the transition layer in the inversion category over EEP during SOP-II. There were 69 soundings with transition layers and 79 soundings without the transition layers.

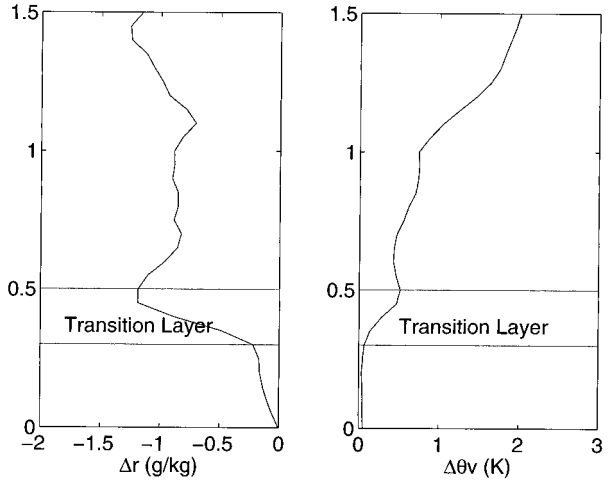

FIG. 10. Differences in θ_v and r between the average soundings with and without the transition layer in the inversion category over EEP during SOP-II. There were 69 transition soundings and 79 nontransition soundings in the inversion category. Here $\Delta\theta_v = \theta_v$(transition) − θ_v(nontransition); $\Delta r = r$(transition) − r(nontransition). Vertical coordinate is the nondimensional height scale where 1 is the base of the trade inversion.

Fig. 8 clearly selects a group of soundings with much lower inversions than the other values of λ.

The θ_v and the r difference between the averaged soundings with the transition layer and those without the transition layer in the inversion sounding group are presented in Fig. 10. The nondimensional height scale was used so that transition structures would be maintained. Transition soundings are clearly drier and warmer in the cloud layer than the nontransition soundings. The differences between the two categories indicate the importance of the transition layer in regulating cloud properties. The virtual potential temperature difference just above cloud base is about 0.5 K and would further inhibit the penetration of turbulent eddies in the subcloud layer to the cloud layer above. This 0.5 K difference acting through a 50-mb layer at cloud base would add about 8 J kg^{-1} to the convective inhibition energy (Williams and Reno 1993) experienced by a parcel originating in the subcloud layer. A nonentraining parcel with an upward motion of 4 m s^{-1} would be required to penetrate such a layer or 2.8 m s^{-1} for a 25-mb layer. Thus this layer can have a substantial impact on the initiation of cumulus elements by turbulent eddies in the subcloud layer.

The increased temperature and the decreased moisture in the cloud layer indicate a decrease in the cloud layer relative humidity. The average relative humidity in cloud layers for the inversion transition soundings is 79% compared with 85% for the inversion soundings with no transition layer. Although this difference is small, it may affect the mean fractional area covered by boundary layer clouds. If the RH-based fractional cloudiness suggested by Albrecht et al. (1995b) is applied to these relative humidity values, the predicted cloud amount is 22% for the transition layer soundings compared with the 34% for the soundings without transitions layers. In the subcloud layer, the differences in r and θ between the two averaged soundings are small. The processes responsible for forming the transition layer have their largest effects above the subcloud layer.

The average bases of the trade wind inversion for soundings with and without the transition layer over the eastern equatorial Pacific during SOP-II were 844 and 868 mb, respectively. The 24-mb difference between them is statistically significant at the 99% level (one-tailed z test, $\alpha = 0.01$, with 79 and 69 soundings in the two categories, respectively). Thus transition layers were observed more frequently in slightly deeper boundary layers. This is also evident from the results shown in Fig. 8 for composite soundings obtained using different values of λ. One possibility for explaining the formation of the transition layer is that if the boundary layer is deepening but the turbulent kinetic energy production does not change, at some point the turbulent kinetic energy may be unable to sustain internal circulations through the whole depth of the deeper boundary layer, and decoupling will occur. Bretherton and Wyant (1997) suggest that decoupling of the boundary layer associated with stratocumulus clouds can be inferred when the negative buoyancy fluxes below cloud base increase to the point where internal circulations cannot sustain mixing through the depth of the boundary layer.

The SST distribution relative to the locations of soundings with and without the transition layers give no evidence that soundings with transition layers are more prevalent over warmer SSTs. Furthermore, the average SST for soundings that have no transition layers in the inversion category is 0.5°C greater than of soundings that have transition layers. The average wind speed and mixing ratio at 980 mb for these two groups are nearly the same. This suggests that the surface sensible and latent heat fluxes associated with the nontransition layer soundings are greater than those for the transition soundings.

4. Comparisons of MABL structures over the cold tongue and the ITCZ

During FGGE the equatorial cold tongue over the eastern Pacific extended from 90°W to about 150°W between 2.5°S and 2.5°N, and the ITCZ was between 5°N to about 10°N. To study the east–west variations over the cold tongue and the ITCZ, these two areas were divided by 2.5° long intervals into 24 rectangular boxes. Soundings in these boxes were then averaged to give E–W cross sections of mixing ratio and potential temperature.

East–west sections of mixing ratio over the cold tongue and the ITCZ are shown in Fig. 11. There is little E–W variation in the water vapor content, although areas over the cold tongue clearly have lower water content than

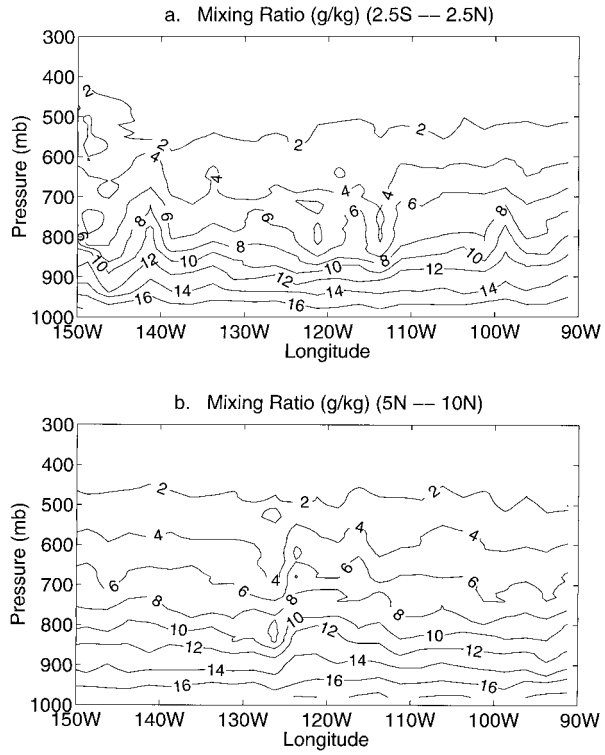

FIG. 11. East–west cross sections of mixing ratio (a) over the cold tongue and (b) over the ITCZ for soundings collected during both SOP-I and SOP-II in FGGE.

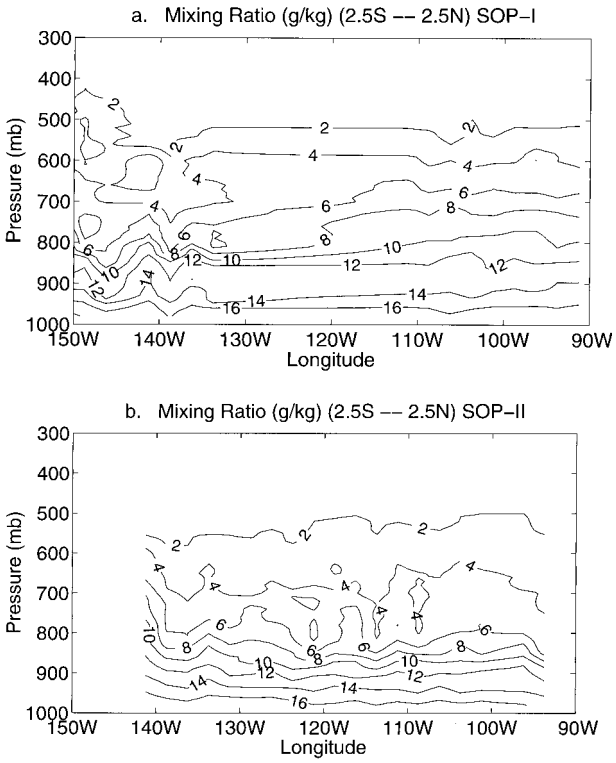

FIG. 12. East–west cross sections of mixing ratio over the cold tongue (a) during SOP-I and (b) during SOP-II.

over the ITCZ. Atmospheric boundary layers in regions west of 140°W over the cold tongue (Fig. 11a) appear slightly more moist since the underlying SSTs are higher in this area compared with areas to the east. The 16 g kg^{-1} contour over the cold tongue (Fig. 11a, about 960 mb) is slightly lower than that over the ITCZ (Fig. 11b, about 940 mb), verifying that the surface layer is more moist over the ITCZ than over the cold tongue. The drying over the cold tongue may be attributed to subsidence associated with the southeasterly trades extending over the cold tongue or from compensating subsidence associated with the deep convection over the ITCZ. From about 115° to 125°W, there is a region of relatively dry air near 800 mb over the cold tongue. Over the ITCZ at this same longitude, the layer from 800 to 500 mb is relatively moist. It is not clear, however, if these cold tongue and ITCZ moisture features are connected. The relatively dry air at 800 mb over the cold tongue may be associated with the area of high OLR (>280 W m^{-2}) south of the equator (Fig. 4). This area is more extensive during SOP-II than SOP-I. The comparison of cross sections of mixing ratio over the cold tongue between SOP-I and SOP-II shown in Figs. 12a and 12b confirms that air from 1000 to 600 mb was substantially drier during SOP-II than SOP-I. The drier air at 115°–125°W that was present in the average SOP-I and SOP-II east–west cross section is associated with SOP-II. The deeper moist layer over the ITCZ at the same longitude is present in the SOP-II cross section (not shown) but not in the SOP-I cross section.

A detailed comparison of the MABL structure over the cold tongue with that over the ITCZ was made by forming composite soundings from these two areas. Figure 13 shows profiles of θ_v, r, θ_e, θ_{es} averaged over all longitudes for the cold tongue and the ITCZ in the eastern equatorial Pacific during SOP-II in FGGE. The two composite soundings are obtained from 1) soundings in the area 10°S–equator and 90°–120°W for the cold tongue (78 soundings), and 2) from soundings in the area 5°–15°N and 90°–120°W for the ITCZ (90 soundings). The temperature and mixing ratio from 980 to 300 mb of the two composite soundings are given in the appendix. The standard deviation profiles corresponding to these mean profiles are shown in Fig. 14. Of significance is the much higher variability in the mixing ratio above 800 mb for the ITCZ sounding and the maximum variability at the top of the boundary layer for both composite soundings.

The potential temperature, mixing ratio, and virtual potential temperature differences between the composite soundings are shown in Fig. 15. The profiles of $\Delta\theta$ indicate that the air from the surface to 800 mb is about 2° warmer in the ITCZ region than over the cold tongue. The average SST for the ITCZ soundings is 28.7°C compared with 26.0°C for the cold tongue. If air at 980 mb in the ITCZ composite soundings were taken adiabat-

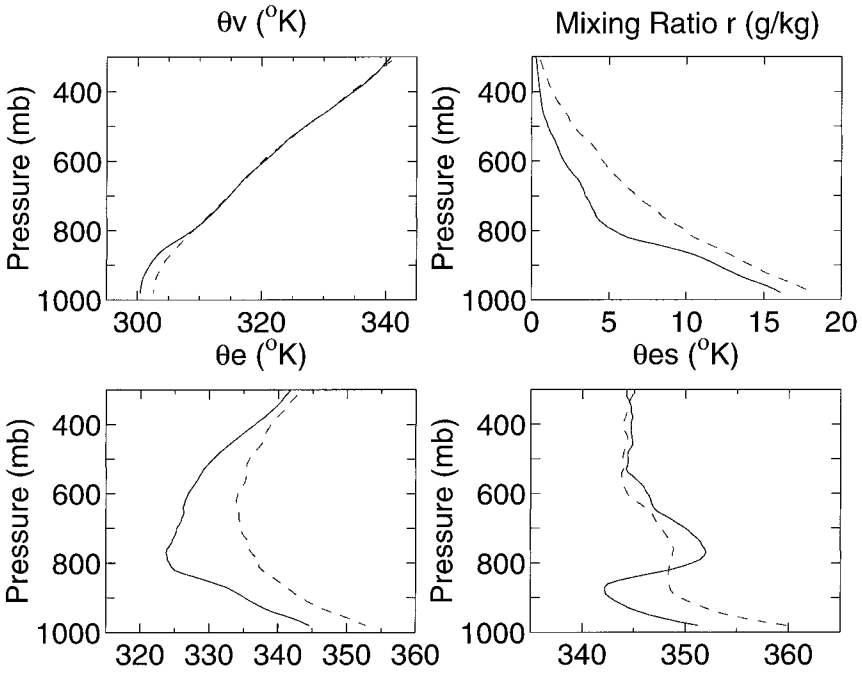

FIG. 13. Averaged profiles of θ_v, r, θ_e, and θ_{es} for soundings over the cold tongue (solid line, 78 soundings) and the ITCZ (broken line, 90 soundings) during SOP-II. The freezing levels of the two averaged soundings are ~560 mb.

ically to 1010 mb, its temperature would be about 0.4°C lower than the average SST. Over the cold tongue, 980-mb air taken adiabatically to 1010 mb would be about 1.1°C lower than the SST. The differences shown in Fig. 15 show little vertical structure from the surface to 800 mb. The cold tongue soundings, however, are slightly warmer (about 0.5°C) than the ITCZ soundings at 800 mb. This temperature difference is consistent with enhanced subsidence over the cold tongue relative to the ITCZ. The profiles of mixing ratio, however, show that the air from the surface to 300 mb over the cold tongue is much drier than in the ITCZ. Transports of moisture

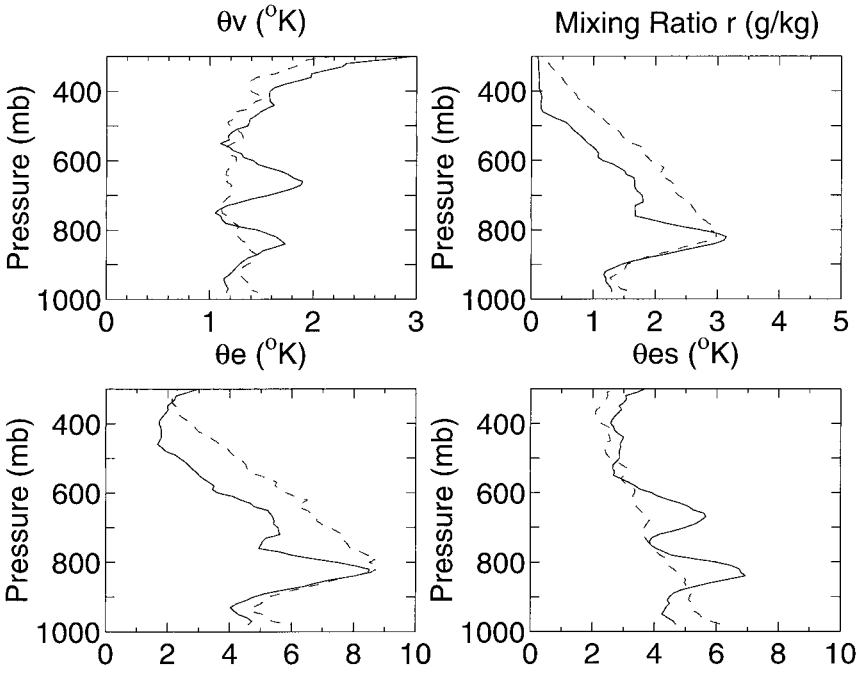

FIG. 14. Standard deviation of variables in Fig. 13.

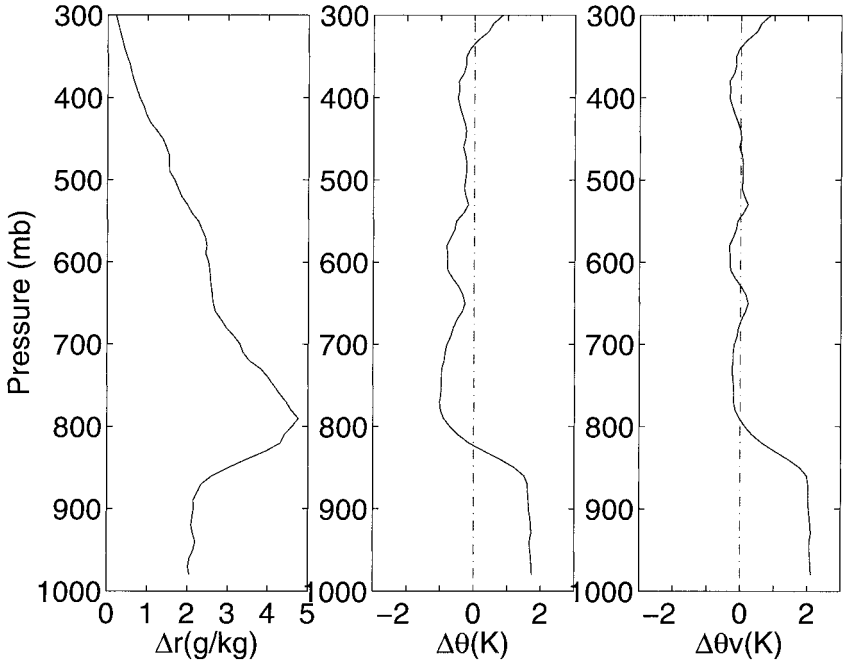

FIG. 15. Differences in θ, r, and θ_v between the ITCZ and the cold-tongue averaged soundings shown in Fig. 13.

to the upper troposphere by convection over the ITCZ and subsidence over the cold tongue are consistent with these differences. Although the mixing ratio and potential temperature differences above 800 mb are significant, the resulting differences in virtual temperature are relatively small. Differences in the low-level stability are further indicated by the profiles of θ_e and θ_{es}. The increased instability over the ITCZ relative to the cold tongue is due to two factors: a higher boundary layer θ_e and the destabilization of the stable layer near 800 mb. A close examination of the composite ITCZ θ_{es} profile over the ITCZ indicates a slightly stable layer at 800 mb that remains in the average since some of the soundings over the ITCZ have inversions at this level.

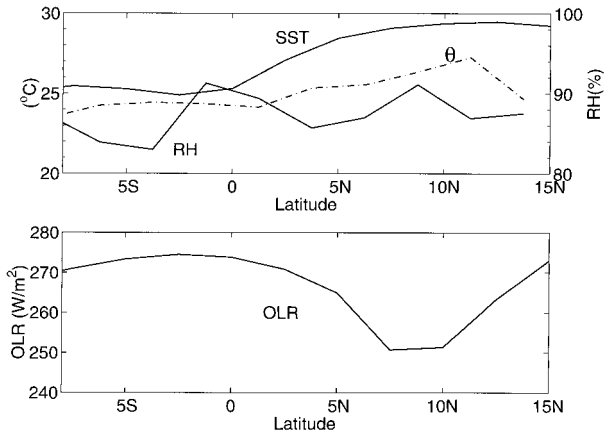

FIG. 16. North–south cross section diagrams of mean SST and OLR as well as RH and θ at 980 mb between 95° and 105°W during both SOP-I and SOP-II.

5. North–south variations in MABL structure over the CTIC

The previous section concentrated on the average thermodynamic differences between the cold tongue and the ITCZ. Here we provide a more detailed description of the latitudinal variations in boundary layer structure over the eastern equatorial Pacific CTIC. This analysis is restricted to SOP-II when the N–S variations in SST were greater than during SOP-I. North–south cross sections for SOP II in two longitudinal bands from 95° to 105°W and from 105° to 115°W were obtained by grouping soundings within the two longitudinal bands into 2.5° latitude intervals. The north–south distributions of the mean SST and OLR for May and June in 1979 along 95°–105°W are shown in Fig. 16. These indicate that the main convective activity indicated by the OLR was located between 8° and 10°N in the eastern equatorial Pacific during FGGE SOP-II with the maximum SST near 12°N. The SST cold tongue was centered at 0°–2°S, although it is not as pronounced as the climatological mean of cold seasons of cold years shown in Wallace et al. (1989). The average RH and θ at 980 mb obtained from the 181 FGGE soundings between 95° and 105°W are also shown in Fig. 16.

The north–south variation of moisture, particularly above 800 mb, is clearly illustrated in Figs. 17a and 17b where the cross sections of mixing ratio over the two longitudinal bands are shown. In both bands there is a well-defined increase in moisture from south to north. A well-defined dry area appears at 800 mb over the equator. This area is also associated with drier conditions near the surface and is located slightly north of

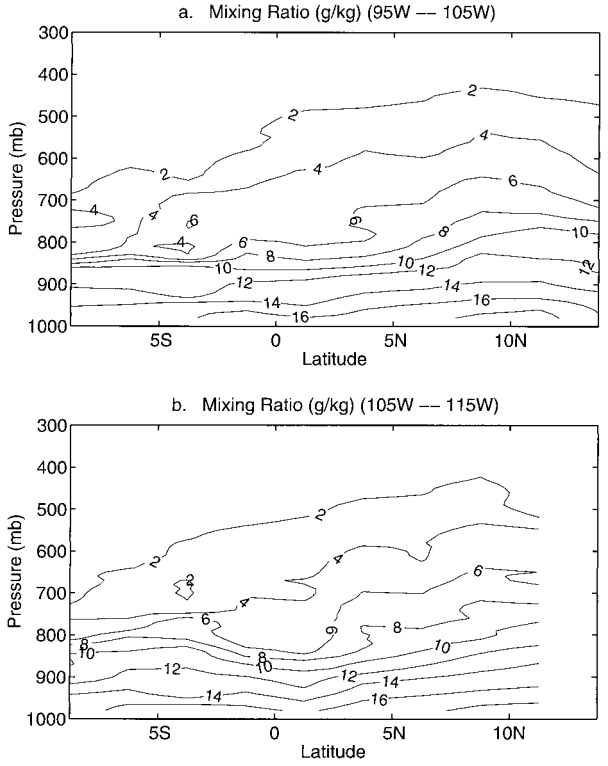

FIG. 17. North–south cross sections of mixing ratio over two longitudinal bands during SOP-II: (a) 95°–105°W; (b) 105°–115°W. The freezing level is located at ~570 mb.

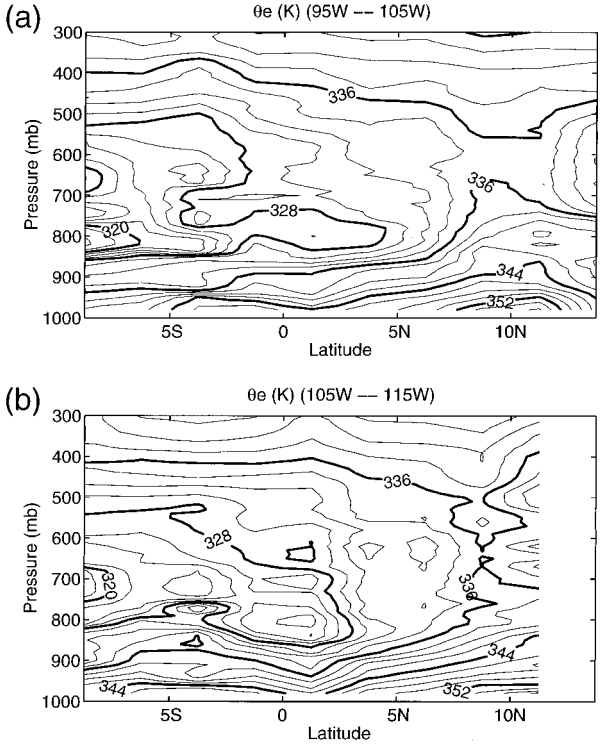

FIG. 18. North–south cross sections of θ_e over the two longitudinal bands during SOP-II: (a) 95°–105°W and (b) 105°–115°W.

the lowest SSTs in this region. Both entrainment of the relatively dry air at 800 mb and reduced surface moisture fluxes over the lower SST regions may contribute to the drying through the boundary layer.

Figure 18 shows north–south cross sections of θ_e over the two longitudinal bands. The dry layer over the equator results in a well-defined minimum in θ_e. The source of the dry air that gives rise to the θ_e minimum is uncertain. Air subsiding in response to upward motion in the ITCZ is one possibility. This would not explain, however, the variations in mixing ratio at 800 mb near the equator since a close examination of the vertical structure shows a relative minimum that is consistent with the mixing ratio reversal discussed by Kloesel and Albrecht (1989). In addition, it is possible that dry air from the South American continent can extend over the eastern equatorial Pacific and influence the cloud properties over the region, although the driest conditions are found in the more westerly of the two longitude bands.

The depth of the boundary layer as indicated by the sharp gradient in θ_e near 800–850 mb shown in Fig. 18 indicates that the heights of the trade inversion layer have little north–south variation except in the 105°–115°W band where the boundary layer is shallowest over the cold tongue. The vertical gradients of θ_e at this level are weaker over the ITCZ, which is consistent with fewer and weaker inversions in this area.

The variations in the meridional and zonal wind component over the eastern equatorial Pacific are shown in Fig. 19. The study domain (EEP shown in Fig. 3) was divided by 2.5° latitude intervals into 10 zones from 95° to 115°W. The mean winds shown in Fig. 19 indicate that from 980 to 920 mb the southerly wind component increases substantially from 10°S to 7.5°N with an abrupt shift to light northerlies at 10°N. These observations are consistent with those shown in previous studies (Bond 1992; Wallace et al. 1989) and indicate a strong acceleration of the winds north of the cold tongue. The largest increase in the southerly wind component is from 2.5° to 7.5°N over the region of increasing SSTs in a relatively shallow layer near the surface. There is little evidence, however, to support the hypothesis proposed by Wallace et al. (1989) that the vertical shear of the meridional wind is greater over the cold tongue than over the higher SSTs to the north because of stability differences. The easterly component is strongest south of the cold tongue and on average is weak to the north of the dry tongue at the 800-mb level. Thus these observations do not support the idea that the dry air at this level is advected from over South America.

Over the cold tongue, the relative humidity at 980 mb (Fig. 16) exhibits a maximum. Wallace et al. (1989) suggested that this increased RH is consistent with the increased boundary layer stability over the cold tongue. Although we do not have quantitative estimates of the

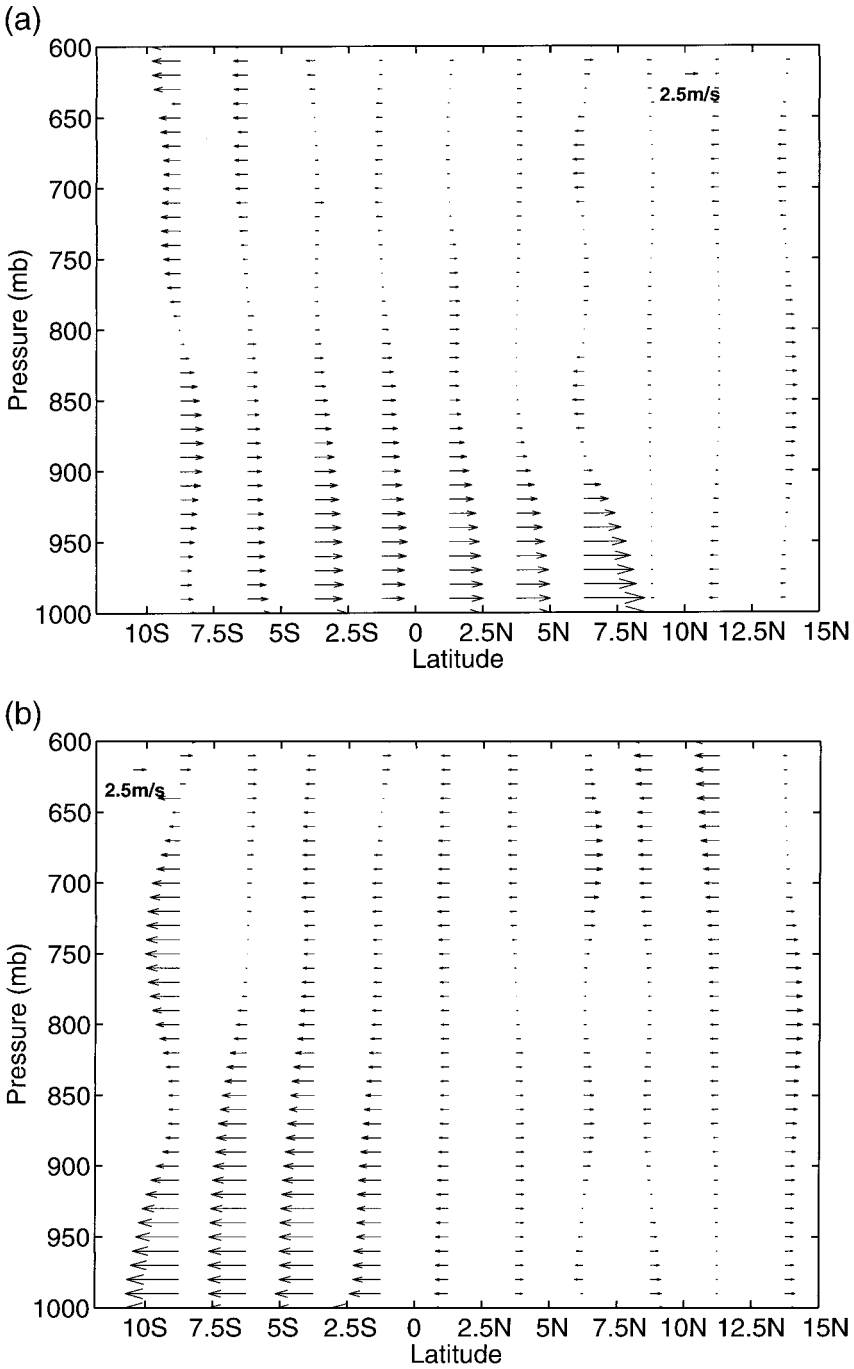

FIG. 19. North–south distribution of the (a) meridional wind component and (b) the zonal wind component over the EEP during SOP-II.

surface fluxes, if the lowest layers are well mixed, the differences between SST and θ at 980 mb imply that the surface sensible heat fluxes north of the equator are greater than those south of the equator. The greatest fluxes would be near 7.5°N, where the winds are strongest and the air–sea differences are large.

The north–south distributions of heights of inversion layers, transition layers, and the LCLs calculated from temperature and mixing ratio at 980 mb are shown in Fig. 20. The inversion heights show a systematic lowering from 10°S to 5°N with an increase over the warmer SSTs. The latitudinal variations in the inversion height over the ITCZ are less reliable since the number of soundings is relatively small at these latitudes.

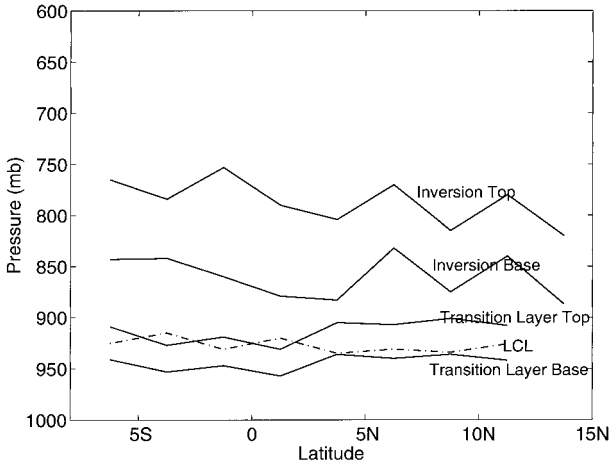

FIG. 20. Latitudinal variations in heights of the inversion, transition layer, and LCLs over EEP during SOP-II.

The average LCLs shown in Fig. 20 are consistently within the transition layer and slightly lower over the ITCZ. This lowering of the LCL over the ITCZ occurs since moistening of the subcloud layer is sufficient to counteract an increase in the LCL associated with the warming. As the LCL is lowered to the base of the transition layer over the ITCZ, one would expect the convective transports to be enhanced since updrafts in the subcloud layer can increase their temperature through latent heat release once they reach the LCL. The trade inversions that are observed over the ITCZ region are not substantially higher than those observed elsewhere, although the frequency of occurrence is substantially reduced. The average inversion height does not increase substantially as air flows over the equatorial front. This region is often associated with low-level stratiform clouds (Deser et al. 1993). These clouds are often attributed to the increased heat and moisture fluxes from the surface. Although the situation may be similar to those observed in cold-air outbreaks in midlatitudes, the clouds may differ substantially in character from those observed in midlatitudes where a relatively deep mixed layer can be maintained by very strong surface fluxes (Mahrt and Paumier 1984). Since a number of the soundings over the higher SSTs have transition layers, it is likely that conditions in this region are often associated with cumulus rising into stratus. This inference is consistent with the ship-based cloud climatologies for this region (Norris 1998).

6. Summary and discussion

Soundings collected during FGGE have been used to study the boundary layer structure over the eastern equatorial Pacific, an area for which there have been few observations of boundary layer structure. In the eastern equatorial Pacific the 453 soundings remaining after a data quality control procedure was applied have been classified into three categories—stable, inversion, and unstable—on the basis of the low-level stability. Approximately 60% of the soundings over the eastern equatorial Pacific during FGGE are found with low-level inversion layers. The inversion layers had an average base at about 850 ($\pm$55) mb and an average top at about 770 ($\pm$63) mb. Stable soundings also had a higher mean LCL than unstable soundings (918 mb as compared with 938 mb). Inversion layers were present in more than 80% of the soundings from 7.5°S to the equator, while more than 40% of the soundings from 2.5° to 12.5°N were found to be unstable.

Although the inversions at 800 mb may be critical in limiting the development of deep convection, the transition layer may represent an important control on the convective coupling between the subcloud and the cloud layer. Transition layers are found to be present in 45% of the soundings over the eastern equatorial Pacific. The mean heights of the bases and the tops of the transition layers are 943 ($\pm$19) mb and 914 ($\pm$24) mb, respectively, and show little spatial or temporal variation. LCLs ($\sim$930 mb) of the soundings with transition layers were always located in the transition layer, consistent with the GATE findings (Fitzjarrald and Garstang 1981). In the regions where more unstable soundings were observed, the LCLs were on average close to the base of the transition layer. Under stable conditions the mean LCL is closer to the top of the transition layer. Transports from the subcloud to the cloud layer may be enhanced when the LCL is close to the base of the transition layer since thermals in the subcloud layer have a higher probability of reaching their condensation level before encountering the stable layer. A comparison between the composite soundings with and without the transition layer indicated that the cloud layers of the transition soundings are drier and warmer than the cloud layer of the nontransition soundings. A layer-by-layer averaging procedure was used to preserve the structure of soundings with both the inversion and the transition layers for this comparison. The drier conditions in the cloud layer are consistent with a decreased transport from the subcloud layer when the transition layer is present. The locations and associated SSTs of soundings with and without the transition layer give no evidence that the transition layer occurs more frequently over warm SSTs. The average difference in virtual potential temperature across the transition layer for different regions and both SOP-I and SOP-II was remarkably constant at 0.9 K. Since the transition layer is an important part of the MABL structure over the eastern Pacific, the processes involved in the formation and maintenance of this layer need further investigation.

We made a detailed comparison of the thermodynamic structure over the cold tongue and the ITCZ north of the equator. The presence of 800-mb inversions is the most obvious feature associated with the cold-tongue soundings. Although most of the soundings in the ITCZ are unstable, more than 30% of soundings in this region

had a stable boundary layer structure. The boundary layers with inversions in the ITCZ may be maintained by subsidence in the vicinity of deep convection. Little east–west variation in the atmospheric structure is observed, although the driest air over the cold tongue at 800 mb is observed between 115° and 125°W.

A comparison of the average thermodynamic structure over the ITCZ with that over the cold tongue indicates that the virtual potential temperature difference between these two areas is confined to the layer between 850 mb and the surface. The ITCZ soundings are approximately 2°C warmer than cold-tongue soundings throughout this layer. This difference is consistent with the mean difference in the SSTs between these two regions. Since the effects of the SST variations are reflected by temperature differences that are uniform through the lowest 150 mb, a definition of the boundary layer that extends from the surface to the trade inversion is clearly appropriate. The mixing ratio for the ITCZ composite soundings is greater at all levels than the mixing ratio for the cold-tongue composite. The mixing ratio at the 800–850-mb layer is 4–5 g kg^{-1} higher over the ITCZ than over the cold tongue. This same layer is about 1°C colder than the same layer over the cold tongue. The negative correlation between mixing ratio and temperature at this level is consistent with changes in the thermodynamic structure due to vertical velocity variations. Thus surface and boundary layer processes alone cannot explain the thermodynamic differences between the cold tongue and the ITCZ. Variability in the large-scale vertical velocity may also be important. The boundary layer structure provides a critical link between the large-scale motions and the type and extent of convection.

A detailed description of the boundary layer structure of the cold tongue–ITCZ complex (CTIC) was made by constructing north–south cross sections (10°S–15°N) of potential temperature, mixing ratio, equivalent potential temperature, and meridional winds for longitudinal bands 95°–105°W and 105°–115°W. The north–south structure in both bands is similar and shows a sharp transition in the meridional winds and the thermodynamic structure at 7.5°N. Inversion heights are slightly lower over the cold tongue than over regions to the north and south. There is little latitudinal variation in the height of the transition layer across the CTIC. Although the LCL of 980-mb air is located near the average top of the transition layers observed over the cold tongue, in the ITCZ it is closer to the average base of the transition layers. These differences, while subtle, may have a substantial impact on the coupling between the subcloud and the cloud layer.

The overall features of N–S variation in the MABL structure over the CTIC as defined from the FGGE dropwinsondes are consistent with structure defined by Bond (1992) in a study that used a much smaller dataset. There was, however, little evidence to support the hypothesis that vertical shear of the meridional wind is greatest over the cold tongue in association with the more stable boundary layer conditions there. The north–south sections indicate that the dry air over the 800-mb inversions (Kloesel and Albrecht 1989) is most pronounced over the cold tongue. A signature of this above-inversion dry air is detected in the boundary layer. This signature indicates that the effects of the dry layer are communicated to the boundary layer through entrainment. The dry layer may be due in part to compensating subsidence associated with convection in the ITCZ as well as the subsidence in divergent southeastern trade winds.

This study indicates little N–S variability of the inversion heights across the CTIC. The theoretical study of Schubert et al. (1995) suggests that the subtropical inversion height is dynamically extended into the Tropics in such a way that there is little variation in the depth of the boundary layer. However, the constancy of the inversion height over the ITCZ itself may also be a manifested by compensating subsidence in the vicinity of deep convection. One way of evaluating the performance of models of the CTIC atmospheric structure will be to examine how well they represent the 800-mb inversions and the variations of these structures across the CTIC. It will be more difficult, however, to make a similar evaluation of the models using transition layer statistics since it is doubtful that large-scale and mesoscale models will ever have the capability to represent transition layer structures. Transition layer structures are an explicit feature of the cumulus parameterizations described by Betts (1973) and Arakawa and Schubert (1974). The stable transition layer at cloud base is also explicitly related to the cumulus dispatcher function first described by Ooyama (1971). Thus a better understanding of how this layer is formed and maintained may be needed to improve parameterizations.

This study was made possible by a unique set of observations that provide an unprecedented description of the thermodynamic structure over the Pacific. But soundings used in this study were mainly used to provide observations in support of data assimilation studies made as a part of FGGE. Consequently, there were relatively few supporting observations that could be used to study processes in the study area. Thus the utility of this dataset is limited. Future monitoring and field studies in this region are being planned as part of the Eastern Pacific Investigation of Climate Processes in the Coupled Ocean–Atmosphere System. These studies should provide the detailed observations of boundary structure over the CTIC.

Acknowledgments. We thank Dr. Chidong Zhang for kindly providing the SST and the OLR data used in this study and Dr. Frank D. Marks for his valuable comments on this project. The helpful comments and constructive criticisms from Dr. Bjorn Stevens and two anonymous reviewers were invaluable for the revision of our original submission. This research was supported by the

APPENDIX

TABLE A1. The average temperature and mixing ratio from 300 to 980 mb for soundings over the cold tongue (10°S to the equator, 90°–120°W) and over the ITCZ (5°–15°N, 90°–120°W). There are 78 and 90 soundings over the cold tongue and the ITCZ during SOP-II, respectively.

	Cold tongue		ITCZ	
Pressure (mb)	Temperature (°C)	Mixing ratio (g kg^{-1})	Temperature (°C)	Mixing ratio (g kg^{-1})
300	−31.5	0.25	−30.9	0.46
350	−22.5	0.38	−22.7	0.86
400	−15.5	0.52	−15.9	1.32
450	−9.7	0.69	−9.9	2.05
500	−5.0	1.06	−5.2	2.73
550	−0.7	1.57	−1.1	3.82
600	3.4	2.06	2.7	4.59
650	6.9	2.96	6.6	5.59
700	10.6	3.46	9.8	6.76
710	11.2	3.63	10.4	7.01
720	11.8	3.76	11.0	7.30
730	12.5	3.84	11.6	7.67
740	13.0	3.98	12.2	7.98
750	13.6	4.09	12.7	8.23
760	14.1	4.16	13.2	8.44
770	14.6	4.34	13.7	8.79
780	15.1	4.61	14.1	9.18
790	15.4	4.88	14.6	9.64
800	15.7	5.30	15.0	9.90
810	15.9	5.68	15.4	10.10
820	16.0	6.19	15.8	10.50
830	16.0	6.99	16.3	10.94
840	15.9	7.99	16.7	11.47
850	16.0	8.90	17.1	11.92
860	16.1	9.75	17.5	12.36
870	16.4	10.49	17.9	12.84
880	16.8	11.03	18.4	13.28
890	17.3	11.56	18.8	13.70
900	17.8	11.99	19.4	14.15
910	18.3	12.44	19.9	14.57
920	18.9	12.92	20.5	15.02
930	19.4	13.41	21.1	15.55
940	20.0	13.92	21.6	16.12
950	20.6	14.58	22.3	16.72
960	21.3	15.18	23.0	17.24
970	22.0	15.69	23.7	17.70
980	22.7	16.08	24.5	18.13

National Oceanic and Atmospheric Administration (NOAA) under Grants NA37RJ0200 and NA67RJOK19.

REFERENCES

Albert, L., 1946: Atmospheric cross-sections of the stratus zone of the tropical Eastern Pacific Ocean. *Trans. Amer. Geophys. Union,* **27,** 800–813.

Albrecht, B. A., C. S. Bretherton, D. Johnson, W. H. Schubert, and A. S. Frisch, 1995a: The Atlantic Stratocumulus Transition Experiment—ASTEX. *Bull. Amer. Meteor. Soc.,* **76,** 889–903.

——, M. P. Jensen, and W. J. Syrett, 1995b: Marine boundary layer structure and fractional cloudiness. *J. Geophys. Res.,* **100,** 14 209–14 222.

Arakawa, A., and W. H. Schubert, 1974: Interaction of a cumulus ensemble with the large-scale environment: Part I. *J. Atmos. Sci.,* **31,** 674–701.

Augstein, E., H. Schmidt, and F. Ostapoff, 1974: The vertical structure of the atmospheric planetary boundary layer in undisturbed trade winds over the Atlantic Ocean. *Bound.-Layer Meteor.,* **6,** 129–150.

Betts, A. K., 1973: Non-precipitating cumulus convection and its parameterization. *Quart. J. Roy. Meteor. Soc.,* **99,** 178–196.

——, 1976: Modeling subcloud layer structure and interaction with a shallow cumulus layer. *J. Atmos. Sci.,* **33,** 2363–2382.

——, and B. A. Albrecht, 1987: Conserved variable analysis of the convective boundary layer thermodynamic structure over the tropical oceans. *J. Atmos. Sci.,* **44,** 83–99.

Bohren, C., and B. Albrecht, 1998: *Atmospheric Thermodynamics.* Oxford University Press, 403 pp.

Bond, N. A., 1992: Observations of planetary boundary-layer structure in the eastern equatorial Pacific. *J. Climate,* **5,** 699–706.

Bretherton, C. S., and M. C. Wyant, 1997: Moisture transport, lower tropospheric stability, and decoupling of cloud-topped boundary layers. *J. Atmos. Sci.,* **54,** 148–167.

Deser, C., J. J. Bates, and S. Wahl, 1993: The influence of sea surface temperature gradients on stratiform cloudiness along the equatorial front in the Pacific Ocean. *J. Climate,* **6,** 1172–1180.

Emanuel, K. A., 1994: *Atmospheric Convection.* Oxford University Press, 580 pp.

Firestone, J. K., and B. A. Albrecht, 1986: The structure of the atmospheric boundary layer in the central equatorial Pacific during January and February of FGGE. *Mon. Wea. Rev.,* **114,** 2220–2231.

Fitzjarrald, D. R., and M. Garstang, 1981: Vertical structure of the tropical boundary layer. *Mon. Wea. Rev.,* **109,** 1512–1526.

Gruber, A., and A. F. Krueger, 1984: The status of the NOAA outgoing Longwave Radiation Data Set. *Bull. Amer. Meteor. Soc.,* **65,** 959–962.

Hayes, S. P., M. J. McPhaden, and J. M. Wallace, 1989: The influence of sea-surface temperature on surface wind in the eastern equatorial Pacific: Weekly to monthly variability. *J. Climate,* **2,** 1500–1506.

Johnson, R. H., P. E. Ciesielski, and K. A. Hart, 1996: Tropical inversions near the 0°C level. *J. Atmos. Sci.,* **53,** 1838–1855.

Kloesel, K. A., and B. A. Albrecht, 1989: Low-level inversions over the tropical Pacific—thermodynamic structure of the boundary layer and the above-inversion moisture structure. *Mon. Wea. Rev.,* **117,** 88–101.

Latif, M., J. Biercamp, H. von Storch, M. McPheden, and E. Kirk, 1990: Simulation of ENSO related surface wind anomalies with an atmospheric GCM forced by observed SST. *J. Climate,* **3,** 509–521.

Lau, K. M., and P. H. Chan, 1983: Short-term climate variability and atmospheric teleconnections from satellite-observed outgoing longwave radiation. Part I: Simultaneous relationships. *J. Atmos. Sci.,* **40,** 2735–2750.

Lindzen, R. S., and S. Nigam, 1987: On the role of sea-surface temperature gradients in forcing low-level winds and convergence in the tropics. *J. Atmos. Sci.,* **44,** 2418–2436.

Mahrt, L., and J. Paumier, 1984: Heat transport in the atmospheric boundary layer. *J. Atmos. Sci.,* **41,** 3061–3075.

Mechoso, C. R., and Coauthors, 1995: The seasonal cycle over the tropical Pacific in coupled ocean–atmosphere general circulation models. *Mon. Wea. Rev.,* **123,** 2825–2838.

Meehl, G. A., 1990: Seasonal cycle forcing of El Niño–Southern Oscillation in a global, coupled ocean–atmosphere GCM. *J. Climate,* **3,** 72–89.

Neelin, J. D., 1990: A hybrid coupled general circulation model for El Niño studies. *J. Atmos. Sci.,* **47,** 674–693.

Neiburger, M., D. S. Johnson, and C.-W. Chen, 1961: Studies of the structure of the atmosphere over the Eastern Pacific Ocean in the summer. *The Inversion over the Eastern North Pacific Ocean,* Vol. 1, University of California Press, 94 pp.

Nicholls, S., 1984: The dynamics of stratocumulus: Aircraft observations and comparisons with a mixed layer model. *Quart. J. Roy. Meteor. Soc.,* **110,** 783–820.

——, and M. A. LeMone, 1980: The fair weather boundary layer in

GATE: The relationship of subcloud fluxes and structure to the distribution and enhancement of cumulus clouds. *J. Atmos. Sci.*, **37,** 2051–2067.

Norris, J. R., 1998: Low cloud type over the ocean from surface observations. Part II: Geographical and seasonal variations. *J. Climate*, **11,** 383–403.

Ooyama, V., 1971: A theory on the parameterization of cumulus convection. *J. Meteor. Soc. Japan*, **49** (Special Issue), 744–756.

Paluch, I. R., and D. H. Lenschow, 1991: Stratiform cloud formation in the marine boundary layer. *J. Atmos. Sci.*, **48,** 2141–2158.

Reynolds, R. W., and W. H. Gemmill, 1984: An objective global monthly mean sea surface temperature analysis. *Tropical Ocean–Atmos. Newsl.*, **23,** 4–5.

Schubert, W. H., P. E. Ciesielski, C. Lu, and R. H. Johnson, 1995: Dynamical adjustment of the trade wind inversion layer. *J. Atmos. Sci.*, **52,** 2941–2952.

Waliser, D. E., N. E. Graham, and C. Cautier, 1993: Comparison of the highly reflective cloud and outgoing longwave radiation dataset for use in estimating tropical deep convection. *J. Climate*, **6,** 331–353.

Wallace, J. M., T. P. Mitchell, and C. Deser, 1989: The influence of sea-surface temperature on surface wind in the eastern equatorial Pacific: Seasonal and interannual variability. *J. Climate*, **2,** 1492–1499.

Williams, E., and N. Renno, 1993: An analysis of the conditional instability of the tropical atmosphere. *Mon. Wea. Rev.*, **121,** 21–36.

Xu, K., and K. A. Emanuel, 1989: Is the tropical atmosphere conditionally unstable? *Mon. Wea. Rev.*, **117,** 1471–1479.